# Modelling and Robust Control of Hybrid Unmanned Aerial-Underwater Robot in the Presence of Uncertainty

Jay Khatri*
khatri.1@iitj.ac.in
Indian Institute of Technology Jodhpur
Jodhpur, Rajasthan, INDIA

Sandeep Gupta†
sngupta@iitk.ac.in
Indian Institute of Technology Kanpur
Kanpur, Uttar Pradesh, INDIA

Jayant Kumar Mohanta‡
jayant@iitj.ac.in
Indian Institute of Technology Jodhpur
Jodhpur, Rajasthan, INDIA

Santhakumar Mohan§
santhakumar@iitpkd.ac.in
Indian Institute of Technology Palakkad
Palakkad, Kerala, INDIA

## ABSTRACT

A "Hybrid" vehicle is one that has the potential to operate in more than one environment. This work demonstrates a robust backstepping control algorithm for the autonomous transmedia operation of a hybrid unmanned aerial-underwater vehicle in the presence of uncertainty. The simplified mathematical model is considered to depict the entire controller design procedure. The numerical simulation is carried out to demonstrate the proposed control system's efficiency and compare it to existing PID control. The vehicle's transient behaviour is compared in six different transmedia manoeuvres between air and water. The suggested control system is evaluated for stability in aerial manoeuvres and transmedia manoeuvres with respect to the conventional PID algorithm in the MATLAB-Simulink environment to demonstrate the superiority of the proposed algorithm.

## CCS CONCEPTS

• **Computer systems organization → Robotic control**.

## KEYWORDS

Unmanned Aerial-Underwater Vehicle, Robust Backstepping Control, Trajectory Tracking, Altitude Control

**ACM Reference Format:**
Jay Khatri, Sandeep Gupta, Jayant Kumar Mohanta, and Santhakumar Mohan. 2023. Modelling and Robust Control of Hybrid Unmanned Aerial-Underwater Robot in the Presence of Uncertainty. In *Advances In Robotics - 6th International Conference of The Robotics Society (AIR 2023), July 05–08, 2023, Ropar, India.* ACM, New York, NY, USA, 6 pages. https://doi.org/10.1145/3610419.3610463

## 1 INTRODUCTION

Unmanned Aerial Vehicles (UAVs) and Unmanned Underwater Vehicles (UUVs) have garnered a great deal of interest over the last several decades due to their numerous uses depending on their respective operating conditions. They are utilised mostly in military activities. They have also been utilised in non-military applications like mapping, surveying, and farming. However, applications like inspecting bridge pylons, oil platforms, ship hulls, underwater piers, or any partially submerged structure will require a single vehicle capable of operating in both media. Mapping oil spills on beaches, rivers, and lakes or underwater erosion and pollution dispersion can become easier with vehicles that are able to operate in both media. The vehicle's ability to operate on both land and water can help lifeguard rescue efforts. The increasing popularity of UAVs and UUVs has created new opportunities and pushed us to seek goals that were previously deemed impractical or unattainable. This has opened up a new field of study in unmanned vehicle research, such as the creation of vehicles that can operate in diverse conditions. A vehicle that can operate in several environments is referred to as a hybrid vehicle. Engineer Bruce Reid designed the Ried Flying Submarine (RFS-1) in 1960, which was the first air-water hybrid vehicle. During the initial test flight, the single-seater was submerged to a depth of 2 metres and was capable of flying at a height of 10 metres. Numerous researchers have performed outstanding work in the development of Hybrid Unmanned Aerial Underwater Vehicles (HUAUV). In a study of already available architecture platforms in terms of aerial and underwater manoeuvring and hovering capabilities with ease of aerodynamic and hydrodynamic modelling, quadrotors are found to be superior to fixed-wing aeroplanes, helicopters, blimps, balloons, and bird-like aerial structures, as well as torpedo and ROV-like underwater structures [3]. A PID-based controller is used to model the concept of a quadrotor with two rotor layers, one for aerial flight and the other for underwater manoeuvring [2][4][7]. The "LOON COPTER" prototype demonstrated by Hamzeh Alzu'bi at el [1] is capable of manoeuvring in both air and water utilising a buoyancy control method. However, this prototype was controlled remotely. In 2015, Maia's team will use PD control to demonstrate a prototype NAVIATOR that can be operated remotely. The NAVIATOR features a two-layer quadrotor design with all rotors operating in both environments. The work is then expanded to construct a control method employing a quaternion-based controller to prevent singularity, a problem during manoeuvring[5][6][8][9]. All of these models were either remotely controlled or semi-autonomous, meaning that location and


*AIR 2023, July 05–08, 2023, Ropar, India*

ACM ISBN 978-1-4503-9980-7/23/07…$15.00
https://doi.org/10.1145/3610419.3610463

altitude were under autonomous control and attitude was under remote controller control. Due to a lack of attention to disruption, this was unable to achieve a smooth transition across media. All of the aforementioned control methods for water-to-air transition are in "floating first and then takeoff" mode, resulting in a longer water-to-air transition settling period. Complete autonomy requires attitude control, therefore, a robust backstepping control algorithm is presented and its simulation output is compared with that of a PID control algorithm.

## 2 PRELIMINARIES

In general, there are certain differences between the mathematical model of the system and the real system. The controller should handle these uncertainties in the system's parameters. In a different scenario, the settings of the system might potentially change while it is in use, influencing the performance that is desired. One definition of matched uncertainty is an input that uses the same path as the control signal. Take a nonlinear system into consideration as follows:

$$\dot{x} = A(x) + B(x)u + \Delta(x,t)$$

Where $A$ and $B$ represent the nominal system functions (known) and the bounded uncertain function is represented by $\Delta$. Let us assume $g(x)$, a known function for which $|\Delta(x,t)| \leq g(x)$. If $\Delta(x,t)$ is considered such as:

$$\Delta(x,t) = B(x).\bar{\Delta}(x,t)$$

This expression is the matching condition for a function of unknown value $\bar{\Delta}$. It is possible to recast the system as:

$$\dot{x} = A(x) + B(x)(u + \bar{\Delta}(x,t))$$

## 3 DYNAMICS MODEL AND PROBLEM FORMULATION

Figure (1) depicts a HUAUV's graphical representation. It has a quadrotor layout with two layers of propellers. The top layer contains aerial propellers, responsible for airborne movement, and the bottom layer consists of screw propellers for underwater manoeuvring.

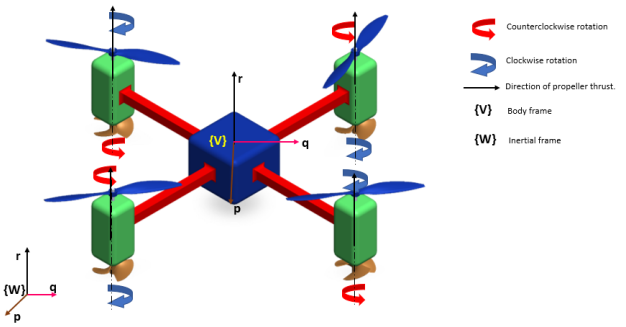


**Figure 1: Pictorial View of HUAUV**

### 3.1 Dynamic Model

The Newton-Euler formulation is used to derive the mathematical model of the proposed HUAUV, with reference to the dynamic modelling of the quadrotor unmanned aerial vehicle, taking into account increased mass, gyroscopic effects, and underwater drag and buoyancy effects. The mathematical model is developed with the assumption that the aerial propellers are responsible for moving in the air, while the screw propellers are responsible for navigating underwater. The intended position influences the choice of the propeller's operating layer close to the water's surface. In addition, the present study focuses on the construction of an algorithm for a seamless transition between aerial and underwater manoeuvring. To minimise excessive complexity, surface manoeuvring is not taken into account; thus, the present model will function as a vertical takeoff and landing device. The whole HUAUV dynamics are presented below[3]:

$$\dot{\mathcal{P}} = v$$

$$m\dot{v} = R_{\zeta}\begin{bmatrix} 0 \\ 0 \\ T_1+T_5 \end{bmatrix} - m\begin{bmatrix} 0 \\ 0 \\ g \end{bmatrix} - \frac{\rho(r)D_{\mathcal{P}}|v|v}{2} \tag{1}$$

$$\zeta = \begin{bmatrix} 1 & \sin\gamma\tan\beta & \cos\alpha\tan\beta \\ 0 & \cos\alpha & -\sin\alpha \\ 0 & \sin\alpha\sec\beta & \cos\gamma\sec\beta \end{bmatrix}\eta$$

$$I\dot{\eta} = l\begin{bmatrix} T_2+T_6 \\ T_3+T_7 \\ T_4+T_8 \end{bmatrix} - \Gamma - \frac{\rho(r)D_{\zeta}|\eta|\eta}{2} - (m+\rho(r)V)gd_e\begin{bmatrix} \sin\alpha \\ \sin\beta \\ 0 \end{bmatrix} \tag{2}$$

where $\mathcal{P}$ and $v$ indicate the location and linear velocity of the HUAUV in the inertial frame $\{W\}$, respectively. $\Omega$ represents the HUAUV's orientation in Specially Orthogonal Matrices SO(3) (in radians) with respect to the inertial frame $\{W\}$. $\eta$ indicates the angular velocity of a HUAUV in relation to its body frame $\{V\}$. $\Gamma$ stands for the gyroscpic effect. Taking into account the small angle approximation, the aforementioned equations (1) and (2) may be revised as follows:

$$\ddot{\alpha} = \dot{\beta}\dot{\gamma}\left(\frac{I_q - I_r}{I_p}\right) + \frac{T_2+T_6}{I_p} - \frac{1}{I_p}(I_r\omega_r + I_{wr}\omega_{wr})\dot{\beta} - \frac{1}{I_p}(m+\rho(r)V)gd_e\sin\alpha - \frac{1}{2I_p}\rho(r)D_{\alpha}|\eta|\dot{\alpha}$$

$$\ddot{\beta} = \dot{\alpha}\dot{\gamma}\left(\frac{I_r - I_p}{I_q}\right) + \frac{T_3+T_7}{I_q} - \frac{1}{I_q}(-I_r\omega_r - I_{wr}\omega_{wr})\dot{\alpha} - \frac{1}{I_p}(m+\rho(r)V)gd_e\sin\beta - \frac{1}{2I_q}\rho(r)D_{\beta}|\eta|\dot{\beta}$$

$$\ddot{\gamma} = \dot{\alpha}\dot{\beta}\left(\frac{I_p - I_q}{I_r}\right) + \frac{T_4+T_8}{I_r} - \frac{1}{2I_r}\rho(r)D_{\gamma}|\eta|\dot{\gamma}$$

$$\ddot{r} = \frac{T_1+T_5}{m}(\cos\alpha\cos\beta) - \frac{1}{m}(m-\rho(r)V)g - \frac{1}{2m}\rho(r)D_r|v|\dot{r}$$

$$\ddot{p} = \frac{T_1+T_5}{m}(\cos\alpha\sin\beta\cos\gamma + \sin\alpha\sin\gamma) - \frac{1}{2m}\rho(r)D_p|v|\dot{p}$$

$$\ddot{q} = \frac{T_1+T_5}{m}(\cos\alpha\sin\beta\sin\gamma - \sin\alpha\cos\gamma) - \frac{1}{2m}\rho(r)D_q|v|\dot{q} \tag{3}$$

In this case, $p, q$, and $r$ indicate the location of the HUAUV in context of the inertial frame $\{W\}$, while $\alpha, \beta$, and $\gamma$ show the orientation of the HUAUV in context of the inertial frame $\{W\}$. The force and moment components of external force, in body frame $\{V\}$, denoted by $T_i$ can be defined as:

$$T_1 = b\left(\omega_1^2 + \omega_2^2 + \omega_3^2 + \omega_4^2\right)$$

$$\begin{bmatrix} T_2 \\ T_3 \\ T_4 \end{bmatrix} = \begin{bmatrix} b\left(\omega_1^2 + \omega_2^2 - \omega_3^2 - \omega_4^2\right) \\ b\left(-\omega_1^2 + \omega_2^2 + \omega_3^2 - \omega_4^2\right) \\ d\left(\omega_1^2 - \omega_2^2 + \omega_3^2 - \omega_4^2\right) \end{bmatrix} \in \mathbb{R}^3 \quad (4\text{-A})$$

$$T_5 = b_w\left(\omega_5^2 + \omega_6^2 + \omega_7^2 + \omega_8^2\right)$$

$$\begin{bmatrix} T_6 \\ T_7 \\ T_8 \end{bmatrix} = \begin{bmatrix} b_w\left(\omega_5^2 + \omega_6^2 - \omega_7^2 - \omega_8^2\right) \\ b_w\left(-\omega_5^2 + \omega_6^2 + \omega_7^2 - \omega_8^2\right) \\ d_w\left(-\omega_5^2 + \omega_6^2 - \omega_7^2 + \omega_8^2\right) \end{bmatrix} \in \mathbb{R}^3 \quad (4\text{-B})$$

Furthermore, in the small vicinity of the water surface, the density varies linearly with respect to altitutde from $\rho_w$ to $\rho_a$ in the range of $-r_c \leq r \leq r_c$ as illustrated in the figure (2).

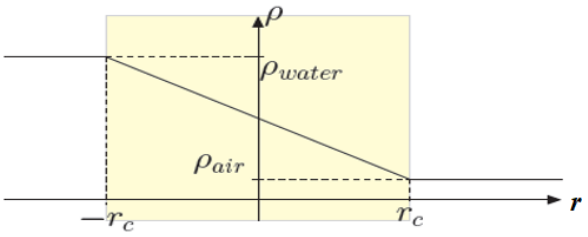


**Figure 2: Density Change near the water surface in a linear manner with the altitude ($r$)**

$$\rho(r) = \begin{cases} \rho_w & \text{if} \quad r < -r_c, \\ \rho_a - \frac{\rho_w - \rho_a}{2r_c}(r - r_c) & \text{if} \quad r_c \leq r \leq -r_c, \\ \rho_a & \text{if} \quad r > r_c. \end{cases} \quad (5)$$

Control inputs $T_1, T_2, T_3, ..., T_8$ needed to be designed to converge all the state tracking errors to converge to zero asymptotically.

## 4 CONTROLLER DESIGN

In this section, three control algorithms are being discussed namely PID, Backstepping, and, in the end, the proposed Robust Backstepping control Algorithm design.

### 4.1 PID Control Design

Figure (3) is a diagrammatic representation of the PID control scheme with gravity compensation. The outer loop is for position control, while orientation is controlled by the inner loop. Equations (6A) and (6B) describe the control laws. Equation (6A) is a generalised control law, whereas Equation (6B) is gain scheduling.

$$T_i = [P][e_i] + [D][\dot{e_i}] + [I][\int e_i dt] \quad (6A)$$

$$[P], [D], [I] = \begin{cases} [P]_w, [D]_w, [I]_w & \text{if} \quad r < 0, \\ [P]_a, [D]_a, [I]_a. & \text{if} \quad r \geq 0 \end{cases} \quad (6B)$$

Here, $[P]$, $[D]$,and $[I]$ are all diagonal matrices, and $e_i$ is the error vector for the variables $p_{ref}$, $q_{ref}$, $r_{ref}$, $\alpha_{ref}$, $\beta_{ref}$, and $\gamma_{ref}$. In order to determine $\alpha_{ref}$ and $\beta_{ref}$, we use $p_{ref}$ and $q_{ref}$ as references. Figure (3) shows that T is for thrust force and $\tau$ for roll, pitch, and yaw moments.

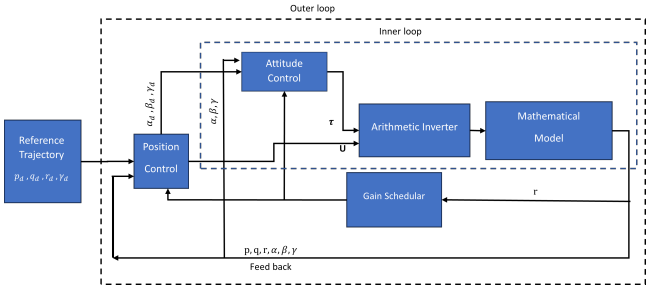


**Figure 3: Proposed Control Scheme with PID**

### 4.2 Backstepping Control Algorithm Design

The backstepping control algorithm presents two control rules, namely virtual control and real control. Taking the altitude subsystem as an example:

$$\dot{r_1} = r_2 \quad (7A)$$

$$\dot{r_2} = F(r) + T_r \quad (7B)$$

Here, from equation (3)
$T_r = \frac{T_1}{m}\cos\alpha\cos\beta \quad and \quad F(r) = -\frac{1}{m}(m - \rho(r)V)g - \frac{1}{2m}\rho(r)D_r|v|\dot{r}$.
The equation for the tracking error is written as $e_{r1} = r_1 - r_{1d}$, and the derivative of this equation is written as $\dot{e}_{r1} = \dot{r}_1 - \dot{r}_{1d} = r_2 - \dot{r}_{1d}$. On the basis of equation (7A), let us assume that the variable $r_2$ is a virtual control input, and moreover, let us assume:

$$r_2 = \dot{r}_{1d} - k_1 e_{r1} \quad (8)$$

Rewriting the derivative of error, $\dot{e}_{r1}$:

$$\dot{e}_{r1} = \dot{r}_{1d} - k_1 e_{r1} - \dot{r}_{1d}, \qquad \dot{e}_{r1} = -k_1 e_{r1} \quad (9)$$

The tracking error $e_{r1}$ will asymptotically converge to zero for $k_1 > 0$. Let's take the expression $e_{r2} = r_2 - r_{2d}$, where $r_{2d}$ may be obtained from equation (8) as follows:

$$r_{2d} = \dot{r}_{1d} - k_1 e_{r1} \quad (10)$$

and

$$e_{r2} = r_2 - \dot{r}_{1d} + k_1 e_{r1} \quad (11)$$

By substituting $\dot{r}_2$ from equation (7B) in the derivative of equation (11), we get the following equation:

$$\dot{e}_{r2} = \dot{r}_2 - \ddot{r}_{1d} + k_1 \dot{e}_{r1} = F(r) + T_r - \ddot{r}_{1d} + k_1 \dot{e}_{r1} \quad (12)$$

If we choose $T_r$ such that,

$$T_r = -F(r) + \ddot{r}_{1d} - k_2 e_{r2} - k_1 \dot{e}_{r1} \quad (13)$$

The simplified error dynamics of equation (12) is expressed as follows:

$$\dot{e}_{r2} = -k_2 e_{r2} \quad (14)$$

We may deduce from equation (14), that if we choose $k_2 > 0$, the tracking error $e_{r2}$ would asymptotically tend towards zero.

A positive definite Lyapunov candidate is selected as follows to analyse the selected subsystem in sense of stability:

$$V = V_1 + V_2 = \frac{1}{2}e_{r1}^2 + \frac{1}{2}e_{r2}^2 \tag{15}$$

Taking the derivative of $V$,

$$\dot{V} = e_{r1}\dot{e}_{r1} + e_{r2}\dot{e}_{r2} = e_{r1}(-k_1 e_{r1}) + e_{r2}(-k_2 e_{r2}) = -k_1 e_{r1}^2 - k_2 e_{r2}^2 \tag{16}$$

For $k_1, k_2 > 0$, $\dot{V}$ will be negative definite, indicating that the subsystem under consideration is stable in the perception of Lyapunov.

## 4.3 Robust Backstepping Control Algorithm Design

The classic backstepping controller is considered ineffective in handling uncertain parameters present in the system dynamics. As a result, we presented a Robust backstepping control, which should function well for the system under consideration.

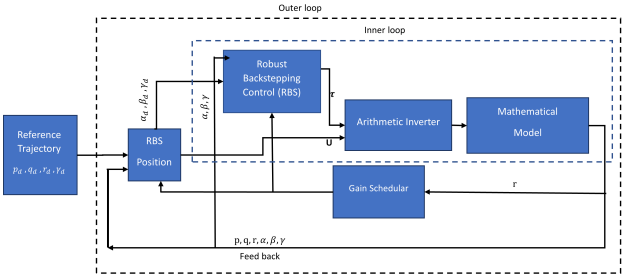


**Figure 4: Proposed Control Scheme with Robust Backstepping**

Let's rebuild the altitude subsystem to include a matched uncertainty of $\Lambda_{mr}$:

$$\dot{r_1} = r_2 \tag{17A}$$

$$\dot{r_2} = F(r) + T_r + \Lambda_{mr} \tag{17B}$$

The tracking error is defined as $e_{r1} = r_1 - r_{1d}$, and its derivative is $\dot{e}_{r1} = r_1 - r_{1d} = r_2 - r_{1d}$. Let us assume a virtual control input $r_2$ from equation (17A) as follows:

$$r_2 = \dot{r}_{1d} - k_1 e_{r1} \tag{18}$$

Rewriting the error derivative $\dot{e}_{r1}$ as:

$$\dot{e}_{r1} = \dot{r}_{1d} - k_1 e_{r1} - \dot{r}_{1d}, \quad \dot{e}_{r1} = -k_1 e_{r1} \tag{19}$$

The error in altiude tracking, denoted by $er1$, will eventually converge to zero for $k_1 > 0$. Let's use the equation $e_{r2} = r_2 - r_{2d}$, where $r_{2d}$ is calculated using equations (18) as:

$$r_{2d} = \dot{r}_{1d} - k_1 e_{r1} \tag{20}$$

and

$$e_{r2} = r_2 - \dot{r}_{1d} + k_1 e_{r1} \tag{21}$$

By substituting $\dot{r}_2$ from equation (17B) in the derivative of equation (21), we get the following equation:

$$\dot{e}_{r2} = \dot{r}_2 - \ddot{r}_{1d} + k_1 \dot{e}_{r1} = F(r) + T_r + \Lambda_{mr} - \ddot{r}_{1d} + k_1 \dot{e}_{r1} \tag{22}$$

If we choose $T_r$ such as:

$$T_r = -F(r) + \ddot{r}_{1d} - k_2 e_{r2} - k_1 \dot{e}_{r1} + \lambda_{mr}, \quad \dot{\lambda}_{mr} = -k_3 \operatorname{sign}(e_{r2}) \tag{23}$$

The error dynamics given by equation (22) can be further reduced to:

$$\dot{e}_{r2} = -k_2 e_{r2} + \Lambda_{mr} + \lambda_{mr} \tag{24}$$

if we adapt $\mu_{mr} = \Lambda_{mr} + \lambda_{mr}$, the equation (24) can be updated as:

$$\dot{e}_{r2} = -k_2 e_{r2} + \mu_{mr}, \quad \dot{\mu}_{mr} = -k_3 \operatorname{sign}(e_{r2}) + \dot{\Lambda}_{mr} \tag{25}$$

if we consider $|\dot{\Lambda}_{mr}| \leq k_3$ and $\mu_{mr} = 0$, the matched uncertainty $\mu_{mr}$ will be wiped out and Hence,

$$\dot{e}_{r2} = -k_2 e_{r2} \tag{26}$$

According to equation (26), $k_2 > 0$ will converge all the tracking error $e_{r2}$ to zero asymptotically. The control rules for position and orientation may be derived by following the identical technique as presented above. A positive definite Lyapunov function is selected for stability investigation as follows:

$$V_r = \frac{1}{2}e_{r1}^2 + k_3 |e_{r2}| + \frac{1}{2}\mu_{mr}^2 \tag{27}$$

Taking the derivative of $V_r$,

$$\dot{V}_r = e_{r1}\dot{e}_{r1} + k_3 \operatorname{sign}(e_{r2})(\dot{e}_{r2}) + \mu_{mr}\dot{\mu}_{mr} \tag{28}$$

and hence,

$$\dot{V}_r = -k_1 e_{r1}^2 + k_3 \operatorname{sign}(e_{r2})[-k_2 e_{r2} + \mu_{mr}] + \mu_{mr}\left[-k_3 \operatorname{sign}(e_{r2}) + \dot{\Lambda}_{mr}\right] \tag{29}$$

Rewritting equation (29) by considering $|\dot{\Lambda}_{mr}| \leq k_3$, $\mu_{mr} = 0$ and $sign(e_{r2})e_{r2} = |e_{r2}|$ such as:

$$\dot{V}_r \leq -k_1 e_{r1}^2 - k_2 k_3 |e_{r2}| \tag{30}$$

According to equation (30), if $k_1, k_2$,and $k_3 > 0$, $\dot{V}_r$ is a bounded and stable function, proving that the subsystem under consideration is stable in the perception of Lyapunov. Hence, it is evident that all the errors converge to zero asymptotically for the proposed algorithm. The same approach outlined above may be used to get the additional control inputs for position and attitude control. The expressions for $T_p$ and $T_q$, equations for position control, can be written as (31 A-B).

$$T_p = -F(p) + \ddot{p}_{1d} - k_{2p}e_p - k_{1p}\dot{e}_p + \lambda_{mp}, \quad \dot{\lambda}_{mp} = -k_{3p} \operatorname{sign}(e_p) \tag{31A}$$

$$T_q = -F(q) + \ddot{q}_{1d} - k_{2q}e_q - k_{1q}\dot{e}_q + \lambda_{mq}, \quad \dot{\lambda}_{mq} = -k_{3q} \operatorname{sign}(e_q) \tag{31B}$$

The expression for attitude control $U_\alpha$, $U_\beta$, and $U_\gamma$ are given in equations (32 A-C).

$$T_\alpha = -F(\alpha) + \ddot{\alpha}_{1d} - k_{2\alpha}e_\alpha - k_{1\alpha}\dot{e}_\alpha + \lambda_{m\alpha}, \quad \dot{\lambda}_{m\alpha} = -k_{3\alpha} \operatorname{sign}(e_\alpha) \tag{32A}$$

$$T_\beta = -F(\beta) + \ddot{\beta}_{1d} - k_{2\beta}e_\beta - k_{1\beta}\dot{e}_\beta + \lambda_{m\beta}, \quad \dot{\lambda}_{m\beta} = -k_{3\beta} \operatorname{sign}\left(e_\beta\right) \tag{32B}$$

$$T_\gamma = -F(\gamma) + \ddot{\gamma}_{1d} - k_{2\gamma}e_\gamma - k_{1\gamma}\dot{e}_\gamma + \lambda_{m\gamma}, \quad \dot{\lambda}_{m\gamma} = -k_{3\gamma} \operatorname{sign}(e_\gamma) \tag{32C}$$

The tracking error $e_i$ can be given as:

$$e_i = i_{measured} - i_{ref}; \tag{33}$$

Where $i = [p, q, r, \alpha, \beta, \gamma]$.
And from equations (3) and (7)

$$F(p) = -\frac{1}{2m}\rho(r)D_p|v|\dot{p} \tag{34A}$$

$$F(q) = -\frac{1}{2m}\rho(r)D_q|v|\dot{q} \tag{34B}$$

$$F(r) = -\frac{1}{m}(m-\rho(r)V)g - \frac{1}{2m}\rho(r)D_r|v|\dot{r} \tag{34C}$$

$$F(\alpha) = \dot{\beta}\dot{\gamma}\left(\frac{I_q - I_r}{I_p}\right) - \frac{1}{I_p}(I_r\omega_r + I_{wr}\omega_{wr})\dot{\beta} - \frac{1}{I_p}(m+\rho(r)V)gd_e\sin\alpha - \frac{1}{2I_p}\rho(r)D_\alpha|\eta|\dot{\alpha} \tag{34D}$$

$$F(\beta) = \dot{\alpha}\dot{\gamma}\left(\frac{I_r - I_p}{I_q}\right) - \frac{1}{I_q}(-I_r\omega_r - I_{wr}\omega_{wr})\dot{\alpha} - \frac{1}{I_p}(m+\rho(r)V)gd_e\sin\beta - \frac{1}{2I_q}\rho(r)D_\beta|\eta|\dot{\beta} \tag{34E}$$

$$F(\gamma) = \dot{\alpha}\dot{\beta}\left(\frac{I_p - I_q}{I_r}\right) - \frac{1}{2I_r}\rho(r)D_\gamma|\eta|\dot{\gamma} \tag{34F}$$

## 5 RESULTS AND DISCUSSION

The simulation is carried out on MATLAB Simulink for the mathematical model proposed in section 3.1. Values of all the necessary system parameters that are required for simulation are provided in the table (1). Here, the system is modelled as having a negatively buoyant configuration. The gain parameters of the proposed backstepping controller are chosen as $k_1 = 2, k_2 = 3, k_3 = 1.5$ and model uncertainty is considered as $0.02 + 0.2sin(t)$.

### 5.1 Aerial Operation

For the aerial operation, simulations are performed to track a desired trajectory, considering uncertainty in the mathematical model. Figure (5) shows that HUAUV can track an eight-shape trajectory perfectly, even in the presence of uncertainty. The aerial simulation is carried out to analyse the stability of the proposed algorithm with `Eight` "8" Shape manoeuvring.

### 5.2 Aerial and Underwater Operations

Simulations are used in airborne and underwater operations to fulfil the job of transient movement. The model is simulated for six different moves between air and water during a 3000-second period, and the results for transient simulation are displayed in the figures (6) and (7). The first 1200 seconds represent the simulation of the HUAUV from air to water and water to air with varied beginning and terminal positions and methods of reaching out. The time between 1200 and 1500 seconds represents the HUAUV's landing on the water's surface, while the time between 1500 and 2500 seconds is used to replicate the diving operation from the surface and the surfacing operation from the underwater move. The last 500 seconds imitate takeoff from the water's surface. It is also discovered that while simulating lifting off from underwater or from the water's surface to air, a substantial overshoot in the HUAUV's height is seen due to the inherent adhesive characteristic of the water molecules. The occurrence of this overshoot in PID verifies the mathematical model under consideration. On the other hand, the suggested Backstepping control law reduces overshoot since the proposed algorithm can swiftly overcome any disturbance to establish a steady response and cancel out the tracking error. Figures (6) and (7) depict the planned trajectory tracking of

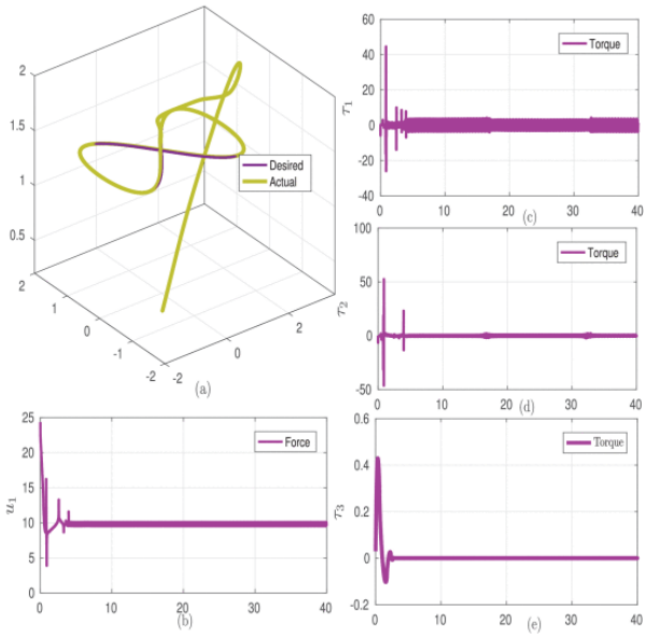


**Figure 5: Results of desired trajectory tracking performance of HUAUV in the aerial operation mode**

HUAUV performance utilising PID and the suggested backstepping controller.

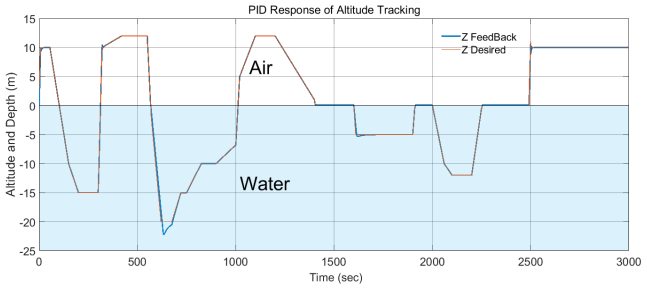


**Figure 6: The trajectory tracking performance of a HUAUV for airborne and underwater operations (PID Algorithm)**

## 6 CONCLUSION AND FUTURE WORK

### 6.1 Conclusion

Six manoeuvres have been identified to handle the challenge of smooth media transitions between water and air in the context of uncertainty: (1) Dive from Air to Underwater, (2) Take off from Underwater to Air, (3) Landing from Air to Water Surface, (4) Dive from Water Surface to Underwater, (5) Surfacing from Underwater, and (6) Take off from Water Surface. The simulation is run for 3000 seconds, and the results reveal that the suggested backstepping method performs better even in the presence of uncertainty. While performing underwater to aerial or water surface to aerial flight simulation, a high overshoot is observed because of the surface tension

**Table 1: Parameters for the Simulation**

| Notation | Value | Description |
|---|---|---|
| M | 1.5 | Mass of robot |
| l | 0.27 | Distance between centre of rotor to centre of mass of robot |
| V | 1.3427e-3 | Robot Volumn |
| I | diag[144648.98, 144648.61, 154104.84]$\times 10^{-7}$ | Mass momment of inertia of robot |
| $I_{ar}$ | 0.04439 | Mass moment of inertia for aerial propeller |
| $I_{wr}$ | 0.01 | Mass moment of inertia fo screw propeller |
| g | 9.81 | Gravity |
| $d_e$ | 0.02 | Distance between the centres of gravity and buoyancy. |
| $\rho_a$ | 1.24 | Air density |
| $\rho_w$ | 1000 | Water density |
| $D_{\mathcal{P}}$ | diag[0.016321, 0.016321, 0.02568] | Drag coefficients for linear motion |
| $D_{\zeta}$ | diag[0.004738, 0.004738, 0.009477] | Drag coefficients for angular motion |

*All the data are in SI unit

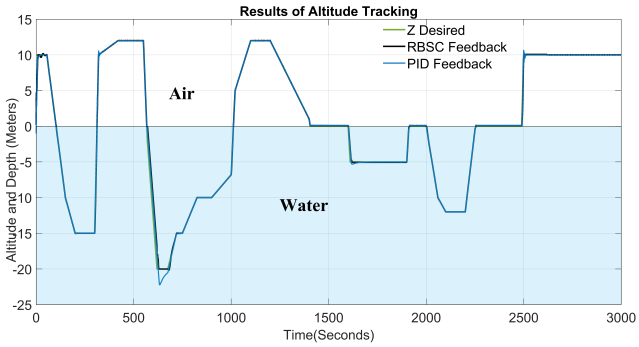


**Figure 7: The performance of the proposed backstepping algorithm for transmedia manoevre in comparison to PID**

and adhesive nature of water particles, which can be substantially minimised by the propsed algorithm. The suggested backstepping controller also minimises the settling time, allowing the robot to reach a stable position more rapidly.

## 6.2 Future Work

The Present work shows a comparative study of the proposed backstepping Algorithm with conventional the PID control algorithm, although the system under consideration lacks a buoyancy mechanism. A stealth buoyancy device is required to increase underwater endurance in idle settings. There is the possibility of modelling the system with a buoyancy mechanism and comparing its performance to the one without a buoyancy mechanism. Furthermore, power consumption may be lowered by optimising the model architecture, indicating that there is still room for development in model design. Furthermore, the selection and design of a buoyancy mechanism is crucial, as it affects the location of gravity centre and buoyancy centre, which ultimately play an important role in maintaining the stable posture for both airborne and underwater mobility. Following the change, we will construct a prototype and test it for trans-media kinematic stability, and the research will be gradually extended to test the prototype in an outdoor situation, taking into account the unpredictability of the environment.

## REFERENCES

[1] Hamzeh Alzu'bi, Iyad Mansour, and Osamah Rawashdeh. 2018. Loon Copter: Implementation of a hybrid unmanned aquatic–aerial quadcopter with active buoyancy control. *Journal of Field Robotics* 35 (8 2018), 764–778. Issue 5. https://doi.org/10.1002/rob.21777

[2] Vivian M Aoki, Pedro M Pinheiro, Paulo L J Drews-Jr, Mauro A B Cunha, and Lucas G Tuchtenhagen. 2021. Analysis of a Hybrid Unmanned Aerial Underwater Vehicle Considering the Environment Transition. *2021 Latin American Robotics Symposium, 2021 Brazilian Symposium on Robotics, and 2021 Workshop on Robotics in Education, LARS-SBR-WRE 2021*, 90–95. https://doi.org/10.1109/LARS/SBR/WRE54079.2021.9605455

[3] Paulo L J Drews, Armando Alves Neto, and Mario F M Campos. 2014. Hybrid Unmanned Aerial Underwater Vehicle: Modeling and simulation. *IEEE International Conference on Intelligent Robots and Systems*, 4637–4642. https://doi.org/10.1109/IROS.2014.6943220

[4] Alexandre C Horn, Pedro M Pinheiro, Ricardo B Grando, Cesar B Da Silva, Armando A Neto, and Paulo L J Drews. 2020. A Novel Concept for Hybrid Unmanned Aerial Underwater Vehicles Focused on Aquatic Performance. *2020 Latin American Robotics Symposium, 2020 Brazilian Symposium on Robotics and 2020 Workshop on Robotics in Education, LARS-SBR-WRE 2020.* https://doi.org/10.1109/LARS/SBR/WRE51543.2020.9307110

[5] D Mercado, M Maia, and F J Diez. 2019. Aerial-Underwater Systems, a New Paradigm in Unmanned Vehicles. *Journal of Intelligent and Robotic Systems: Theory and Applications* 95 (1 2019), 229–238. Issue 1. https://doi.org/10.1007/s10846-018-0820-x

[6] Diego A Mercado, Marco M Maia, and F Javier Diez. 2017. *Aerial-Underwater Systems, a new paradigm in Unmanned Vehicles*.* https://doi.org/10.0/Linux-x86_64

[7] Armando Alves Neto, Leonardo A Mozelli, Paulo L J Drews, and Mario F M Campos. 2015. Attitude control for an Hybrid Unmanned Aerial Underwater Vehicle: A robust switched strategy with global stability. *Proceedings - IEEE International Conference on Robotics and Automation* 2015-June, 395–400. Issue June. https://doi.org/10.1109/ICRA.2015.7139029

[8] Diego Alberto Mercado Ravell, Marco Moreno Maia, and Francisco Javier Diez. 2018. Modeling and control of unmanned aerial/underwater vehicles using hybrid control. *Control Engineering Practice* 76 (1 2018), 112–122. https://doi.org/10.1016/j.conengprac.2018.04.006

[9] Parth Soni, Somaiya Vidyavihar, F J Diez, Marco Moreno, Maia Parth, and Soni F Javier Diez-Garias. 2015. Demonstration of an Aerial and Submersible Vehicle Capable of Flight and Underwater Navigation with Seamless Air-Water Transition. https://www.researchgate.net/publication/279968697